Hindawi
Shock and Vibration
Volume 2019, Article ID 5284194, 13 pages
https://doi.org/10.1155/2019/5284194

Research Article

Analysis of the Vibration Characteristics of a Boring Bar with a Variable Stiffness Dynamic Vibration Absorber

Lie Li, Beibei Sun, and Haitao Hua

School of Mechanical Engineering, Southeast University, Nanjing 211189, China

Correspondence should be addressed to Beibei Sun; bbsun@seu.edu.cn

Received 11 March 2019; Revised 27 June 2019; Accepted 15 July 2019; Published 1 August 2019

Academic Editor: Huu-Tai Thai

Boring bars are widely used in deep hole machining. Due to the low stiffness of the long cantilever boring bar, vibration often occurs in the boring process. Vibration suppression can permit higher productivity and a better surface finish. To improve the performance of boring operations, a variable stiffness dynamic vibration absorber (DVA) is added inside the boring bar to reduce the vibration. The stiffness of the DVA is provided by two rubber bushes placed inside the DVA. By changing the axial compression, the stiffness of the DVA can be adjusted to accommodate different excitation frequencies. By establishing the relationship between the stiffness of the DVA and the axial compression of the rubber bush, the optimal stiffness for different excitation frequencies can always be found. A boring experiment is conducted, and the results show that, by selecting a reasonable axial compression, the vibration of the boring bar can be effectively suppressed.

1. Introduction

Boring bars are widely used in deep hole machining. However, when the boring bar has a large length-to-diameter ratio, vibration often occurs, which leads to a negative impact on the processing quality and processing performance [1, 2]. Passive and active methods can be used to reduce vibration [3–5].

Passive vibration reduction methods have been used in engineering for many years. The earlier scholars mainly focused on the mechanism structures, boring bar materials, and theory of passive damping. Suyama et al. [6] determined that, by using carbide rod materials, boring can accommodate a longer overhang. In addition, the vibration can be reduced by using particle impact dampers. Xia et al. [7] designed a boring bar from a composite material. The composite material can increase the natural frequency, static stiffness, and damping ratio of the boring bar. Cutting experiments indicated that compared to results of the regular boring bar, the amplitude can be reduced by 34%. Sortino et al. [8] illustrated the influence of the boring bar material, geometry, cutting edge geometry, workpiece material, and cutting parameters on process stability in boring. The experimental results showed that the process stability mainly depends on the ratio of the boring bar overhang to the diameter. Houck et al. [9] designed a tuned holder working as a DVA. By matching the natural frequency of the holder to the natural frequency of the boring bar, the stability of the boring bar was increased. Liu et al. [10, 11] designed a novel variable stiffness DVA. The stiffness of the DVA could be changed by changing the overhang length of the DVA. Then, the influences of the excitation frequency and the overhang length of the DVA on the amplitude ratio were discussed, and the optimal curves were obtained. Li and Sun [12] modeled the boring bar as a two-degree-of-freedom system. The stiffness of the DVA was provided by two rubber bushes. The simulation results showed that the stiffness of the DVA consists of the radial stiffness and the shear stiffness of the rubber bushes. Rubio et al. [13] focused on the optimization of the passive DVA parameters. The optimization criterion consisted of the maximization of the minimum values of the stability lobe diagram. The computed results showed a clear improvement in the stability performance. Miguélez et al. [14] modeled the boring bar with a passive DVA as a cantilever Euler beam. The stability was analyzed by constructing a stability diagram, dependent on the boring bar characteristics and on the DVA parameters. Sortino et al. [15] presented a hybrid dynamic model method for boring bars based on empirical models. The model was refined by cutting experiments with different

geometries and materials. The predicted modal parameters were in good accordance with the experimental values. Budak and Ozturk [16] studied the dynamics and stability of a parallel cutting boring bar. The results showed that the dynamic interaction between the parallel tools creates an absorber effect on each other, which increases the stability of the boring process. For the passive vibration reduction method, the biggest problem is poor adaptability. The vibration absorption effect is affected by the DVA parameters and the cutting parameters. Once the cutting parameters change, the DVA is not able to absorb the vibration effectively.

With the development of smart materials, sensing technology, and control technology, active vibration absorption technology has developed rapidly. Yigit et al. [17] studied the effect of piezoelectric shunt damping in the boring process. The electrical impedance was connected to a piezoelectric transducer that is bonded on the boring bar. The effects of optimizing piezoelectric shunt damping on the dynamic stiffness and boring stability were studied experimentally. Abele et al. [18] presented an actively damped boring tool and showed the modeling method of the proposed boring bar. The requirements and the design of the actively damped tool system were discussed. Alammari et al. [19] filled the boring space with fluid and changed the natural frequency of the boring bar based on semiactive fluid control. The mass at the end of the boring bar could be adjusted by changing the level of the fluid. Chen et al. [20–22] designed an active damping boring bar using a magnetic actuator. The actuator was designed to have a linear force output relative to the input current and was used to control the boring bar vibration. Matsubara et al. [23] installed piezoelectric actuators into the boring bar to suppress vibration. An inductor-resister (LR) circuit was designed as a mechanical DVA, and the chatter vibration was successfully suppressed in the cutting test. Compared to the passive vibration reduction method, the active method is more adaptable. Different actuators and control algorithms can be used to reduce the vibration of the boring bar. However, active vibration reduction methods require attachments of sensors and actuators, and the complex structure brings some difficulties in application.

Passive and active vibration reduction methods both have certain defects; however, the passive vibration reduction boring bar is more widely used in engineering, as it has a simple structure and high reliability. As mentioned before, the main problem of the passive vibration reduction method is that it cannot realize the adjustment function for different cutting parameters. In this paper, the boring bar with a variable stiffness DVA is analyzed, and the stiffness of the DVA is provided by two rubber bushes placed inside the DVA. By adjusting the axial compression, the stiffness of the DVA can be adjusted to accommodate different excitation frequencies. By establishing the relationship between the stiffness of the DVA and the axial compression of the rubber bush, the optimal stiffness for different excitation frequencies can always be found.

2. Dynamic Models of Boring Bars

Figure 1 shows the structure of the boring bar with a variable stiffness DVA. The DVA, consisting of a mass block, rubber bush, and damping oil, is placed inside the boring bar. The mandrel is fixed with the boring bar. When vibration occurs, the vibration energy is transmitted from the mandrel to the mass block through the rubber bush and damping oil. When the mass block vibrates and rubs against the damping oil, the vibration energy is consumed.

The dynamic model of the boring bar is established based on the two-degree-of-freedom dynamic model. As shown in Figure 2, the boring bar is subjected to three forces during the cutting process, namely, axial force F_f, tangential force F_c, and radial force F_p. However, the rigidity of the bar is much higher along the feed or axial direction than in the tangential and radial bending directions. On the contrary, the bar exhibits higher stiffness in torsion than in bending. Therefore, the bending vibrations caused by the tangential force F_c and radial force F_p should be considered in the analysis [24]. The excitation force is expressed as follows:

$$\overrightarrow{F_0} = \overrightarrow{F_c} + \overrightarrow{F_p}. \tag{1}$$

To simplify the calculation, the excitation force can be equivalent to a sine wave:

$$F_0 = F\sin(\omega t), \tag{2}$$

where F and ω are the amplitude and frequency of the excitation force, respectively. The dynamic model of the boring bar with variable stiffness DVA can be expressed as follows:

$$\begin{cases} M\ddot{x}_1 + (C+c)\dot{x}_1 + (K+k)x_1 - c\dot{x}_2 - kx_2 = F\sin(\omega t), \\ m\ddot{x}_2 + c\dot{x}_2 + kx_2 - c\dot{x}_1 - kx_1 = 0, \end{cases} \tag{3}$$

where M and K are the equivalent mass and equivalent stiffness of the boring bar, respectively. m, k, and c are the equivalent mass, equivalent stiffness, and equivalent damping of the DVA, respectively.

When the excitation force on the boring bar is expressed as $F_0 = Fe^{j\omega t}$, the displacement of the boring bar can be expressed as

$$x_1 = \overline{X_1}e^{j\omega t}, \tag{4}$$

where $\overline{X_1}$ is the complex amplitude of the boring bar.

By solving equation (3), the complex steady-state amplitude can be obtained as

$$\frac{\overline{X_1}}{F}(\omega) = \frac{-m\omega^2 + k + jc\omega}{[Mm\omega^4 - (Mk + mK + mk + cC)\omega^2 + kK] + j\{-[Mc + m(C+c)]\omega^3 + (cK + Ck)\omega\}}. \tag{5}$$

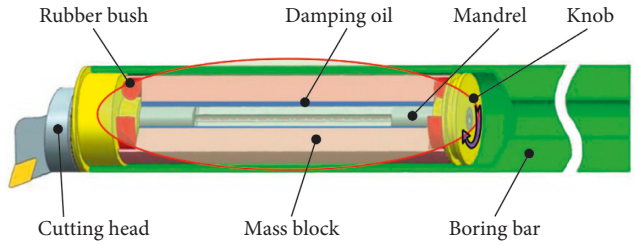

Figure 1: Structure of the boring bar with a variable stiffness DVA.

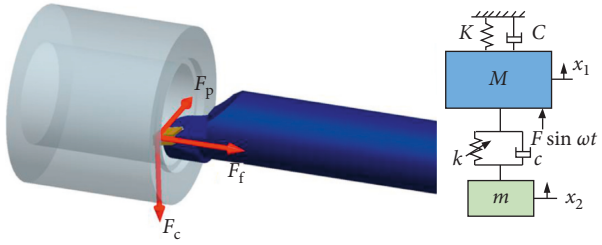

Figure 2: Dynamic model of the boring bar with a variable stiffness DVA.

Then, the real part of the steady-state amplitude can be expressed as

$$\frac{X_1}{F}(\omega) = \frac{\sqrt{(-(m/k)\omega^2+1)^2 + ((c/k)\omega)^2}}{\sqrt{[(Mm/Kk)\omega^4 - ((M/K)+(m/k)+(m/K)+(Cc/Kk))\omega^2+1]^2 + \{-[(M/K)+(m(C/c+1)/K)]\omega^3 + (1+(Ck/Kc))\}^2((c/k)\omega)^2}}. \tag{6}$$

Let $\Omega_n = \sqrt{K/M}$, $\omega_n = \sqrt{k/m}$, $\mu = m/M$, $\zeta = c/2m\omega_n$, $Z = C/2M\Omega_n$, and $X_{st} = F/K$.

The amplitude ratio of the boring bar can be expressed as

$$\frac{X_1}{X_{st}}(\omega) = \frac{\sqrt{\left[-(\Omega_n/\omega_n)^2(\omega/\Omega_n)^2+1\right]^2 + \left[2\zeta(\Omega_n/\omega_n)^2(\omega/\Omega_n)\right]^2}}{\sqrt{\Delta}}, \tag{7}$$

where

$$\Delta = \left\{\left(\frac{\Omega_n}{\omega_n}\right)^2\left(\frac{\omega}{\Omega_n}\right)^4 - \left[(1+\mu)+\left(\frac{\Omega_n}{\omega_n}\right)^2 + 4\zeta\left(\frac{\Omega_n}{\omega_n}\right)^2 Z\right]\left(\frac{\omega}{\Omega_n}\right)^2 + 1\right\}^2 + \left\{-\left(1+\mu+\frac{Z}{\zeta}\right)\left(\frac{\omega}{\Omega_n}\right)^2 + \left[1+\frac{Z}{\zeta}\left(\frac{\omega_n}{\Omega_n}\right)^2\right]\right\}^2 \cdot \left[2\zeta\left(\frac{\Omega_n}{\omega_n}\right)^2\left(\frac{\omega}{\Omega_n}\right)^2\right]. \tag{8}$$

To obtain the parameters of the boring bar, some experimental research was carried out. As shown in Figure 3, the hollow boring bar without a DVA is fixed on a platform with an overhang of 310 mm. The material of the tool bar is steel. A mass block is placed at the end of the boring to provide a load, and the displacement caused by the load can be measured with a micrometer. To improve the accuracy of the measurement, multiple sets of loading values are selected. Figure 4 shows the force-displacement curve. Through a derivation, the stiffness of the boring bar can be obtained.

To obtain the equivalent mass of the boring bar, an impact test is carried out with an impulse hammer, as shown in Figure 5. The frequency response function (FRF) curve of the boring bar (without a DVA) is obtained as shown in Figure 6.

It is clear that the FRF has a distinct peak in the low-frequency area, which corresponds to the first-order bending natural frequency ω of the boring bar. As the stiffness K has already been obtained, the equivalent mass M of the boring bar can be calculated by

$$M = \frac{K}{\omega^2}. \tag{9}$$

The boring bar (without the DVA) can be regarded as a damped single-degree-of-freedom system whose vibration response can be expressed as

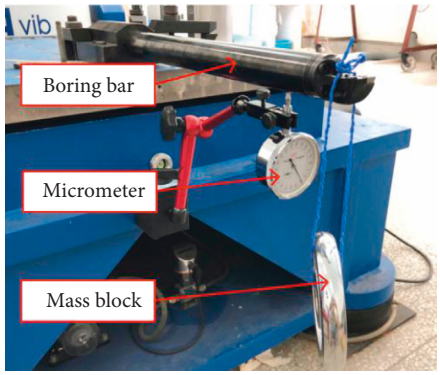

Figure 3: Photograph of a stiffness test of the boring bar.

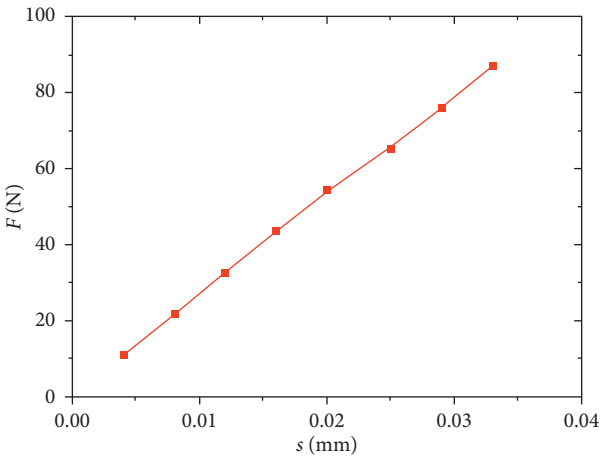

Figure 4: Force-displacement curve of the boring bar.

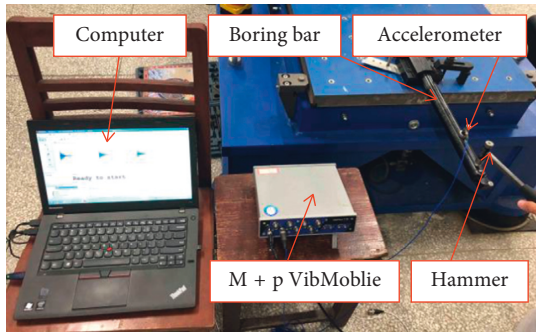

Figure 5: Impact test of the boring bar.

$$x(t) = e^{-\zeta\omega t}\left(x_0 \cos \omega_d t + \frac{\zeta\omega x_0 + v_0}{\omega_d} \sin \omega_d t\right), \tag{10}$$

where ζ is the damping ratio, ω is the undamped natural frequency of the system, ω_d is the damping natural frequency of the system, x_0 is the initial displacement, and v_0 is the initial velocity. Figure 7 is the response curve of free vibration corresponding to formula (10). Using the attenuation ratio between the peak amplitudes, the damping of the system can be calculated.

The attenuation coefficient φ is introduced to characterize the attenuation rate of the vibration amplitude:

$$\begin{aligned}\varphi &= \frac{|A_k|}{|A_{k+1}|} \\ &= \frac{e^{-\zeta\omega t}\left(x_0 \cos \omega_d t + (\zeta\omega x_0 + v_0/\omega_d)\sin \omega_d t\right)}{e^{-\zeta\omega t}\left[x_0 \cos \omega_d (t+T) + (\zeta\omega x_0 + v_0/\omega_d)\sin \omega_d (t+T)\right]} \\ &= \frac{Ae^{-\xi\omega t}}{Ae^{-\xi\omega (t+T)}} = e^{\xi\omega T},\end{aligned} \tag{11}$$

where A_k is the positive amplitude of the kth period, A_{k+1} is the positive amplitude of the $k+1$th period, and T is the vibration period.

Then, the logarithmic attenuation ratio rate is

$$\delta = \ln \varphi = \xi\omega T, \tag{12}$$

$$\xi\omega = \frac{\delta}{T}, \tag{13}$$

where

$$T = \frac{2\pi}{\sqrt{\omega^2 - (\xi\omega)^2}}. \tag{14}$$

Substituting formula (14) into formula (13), we get

$$\delta = \frac{2\pi\xi}{\sqrt{1-\xi^2}}. \tag{15}$$

Then, the damping radio can be calculated as

$$\xi = \frac{\delta}{\sqrt{4\pi^2 + \delta^2}}. \tag{16}$$

The damping constant C of the boring bar can be expressed as

$$C = 2\xi\sqrt{MK} = \frac{2\delta\sqrt{MK}}{\sqrt{4\pi^2 + \delta^2}}. \tag{17}$$

The DVA is also tested by the above method. Table 1 shows the test results. It can be seen that the equivalent stiffness and equivalent mass of the boring bar with DVA are lower than those of the regular boring bar. The main reason is that, in order to place the DVA, a cylindrical cavity is processed at the end of the boring bar. Compared with the response of the regular boring bar, the natural frequency of the proposed boring bar increased from 225.6 Hz to 268.60 Hz. This means that the rigidity of the proposed boring bar is higher, which is beneficial to the stability of the system.

3. Analysis of the Vibration Characteristics of the Boring Bar

By substituting the parameter values in Table 1 into formula (7), the amplitude ratio of the boring bar can be obtained, as shown in Figure 8. The black curve indicates the boring bar

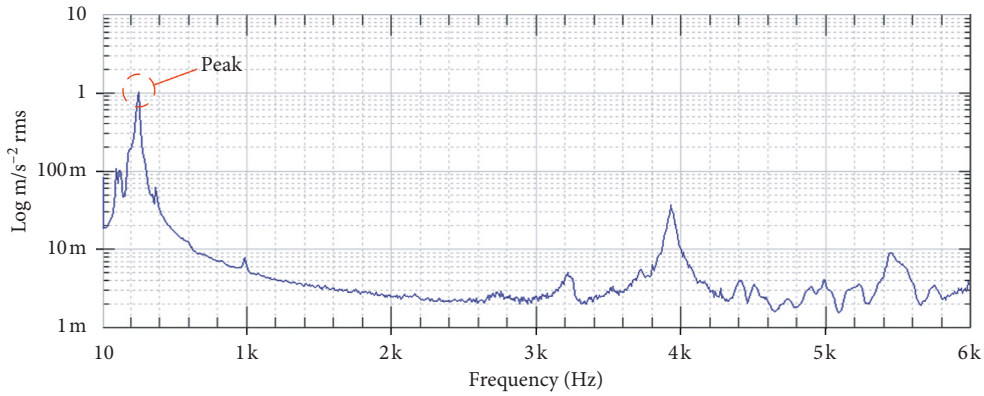

Figure 6: Frequency response function (FRF) curve of the boring bar.

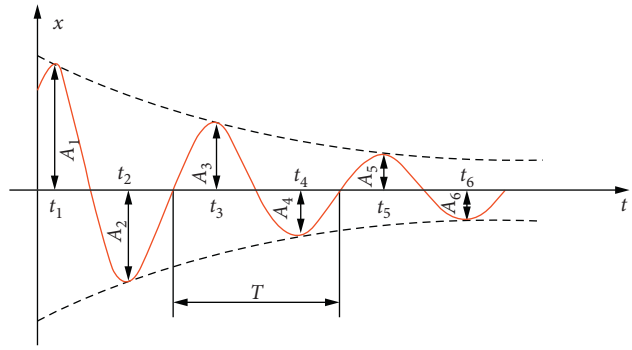

Figure 7: Response curve of free vibration.

Table 1: Parameters of the boring bar with a variable stiffness DVA.

	Equivalent stiffness of the boring bar, K (N/mm)	Equivalent mass of the boring bar, M (kg)	Natural frequency of the boring bar, ω (Hz)	Time period, T (s)	Damping coefficient of the boring bar, C (N·s/m)	Equivalent mass of the DVA, m (kg)	Damping coefficient of the DVA, c (N·s/m)
Boring bar with a DVA	2496.6	0.8764	268.62	0.02339	9.98	0.9126	249.92
Regular boring bar without a DVA	2563.2	1.2757	225.60	0.02785	9.99	—	—

without the DVA, while the red, green, yellow, and blue curves indicate the boring bar with the DVA. For the boring bar without the DVA, the amplitude ratio has only one peak. The amplitude ratio reaches a maximum point when the frequency ratio is approximately 1. At this point, the excitation frequency is close to the natural frequency of the boring bar, which means that the boring bar is working in a resonance state. In addition, when the frequency ratio is less than 1.4, the amplitude ratio of the boring bar (without DVA) is greater than 1, indicating that the vibration amplitude of the boring bar is greater than its static displacement, which means that the frequency range where the boring bar can cut stably is very narrow. By adding the DVA, the boring bar becomes a two-degree-of-freedom system with two peaks. Between the two peaks, an area with an amplitude ratio of less than 1 appears. In other words, the addition of DVA expands the frequency range where the boring can cut stably, which has a positive effect on increasing the stability of the boring bar. With the increasing stiffness of the DVA, both peaks move to the right, and the amplitude ratio of the left peak increases, while the amplitude ratio of the right peak decreases. At the same time, the frequency range between the two peaks where the boring can cut stably is expanded. As an example, when the stiffness of the DVA is $6e^5$ (N/mm), the range of the frequency between the two peaks where the boring can cut stably is 0.50–0.62. When the stiffness reaches $10e^5$ (N/mm), the range of the frequency is expanded to 0.58–0.88. The frequency range is increased by 150% from 0.12 to 0.30. In general, the variable stiffness of the DVA improves the

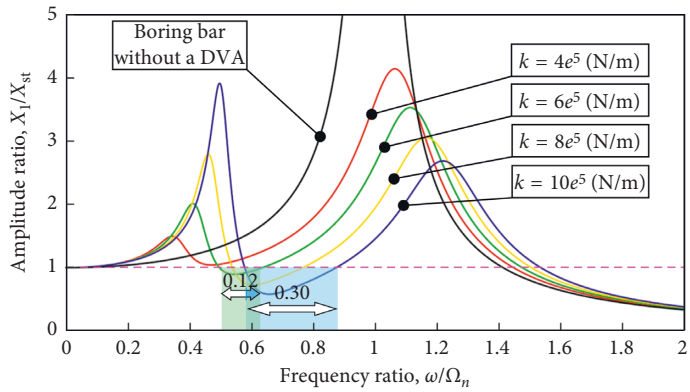

Figure 8: Amplitude ratio of the boring bar under different stiffnesses of the DVA.

stability of the boring bar, and through the selection of different stiffnesses, the boring bar can be adapted to different excitation frequencies.

Figure 9 shows the three-dimensional surface of the amplitude ratio under the influence of the coupling of the frequency ratio and the stiffness of the DVA. The frequency ratio is in the range of 0–2.2, while the stiffness is in the range of $2e^5$–$10e^5$ (N/m). The entire area is divided into two parts: the low-frequency area A and the high-frequency area B. The dividing line is located at a frequency ratio of approximately 1.55. In area B, the excitation frequency is far from the natural frequency of the boring bar, and the amplitude ratio is always below 1, which means that the boring bar can cut stably. Moreover, in area B, with increasing frequency ratio and stiffness, the amplitude ratio decreases. In area A, two ridges can be found where the amplitude ratio is very high; once the boring bar works near the two ridges, the boring bar vibrates violently. Therefore, when the boring bar is working in the low-frequency area A, it is necessary to avoid the two ridges. Fortunately, in the valley between the two ridges, an optimal curve can be found located in the frequency range 0.4–0.8, where the amplitude ratio is less than 1. Therefore, in low-frequency areas, the boring bar's cutting parameters should be selected as close as possible to the optimal curve. Figure 10 shows the amplitude ratio of the optimal curve; most of the curve is below 1, indicating that with reasonable parameter selection, the variable stiffness DVA can play a good role in suppressing vibration in the low-frequency area.

In machining, different cutting parameters, including the cutting speed, cutting depth, and cutting feed, are selected based on different workpiece materials and different quality requirements. Once the cutting parameters are selected, the spindle speed f(r/s) is determined, which means that the main frequency of the excitation force $\omega = 2\pi f$(rad/s) is also determined. At this time, the most important thing is to select the suitable stiffness of the DVA according to the different frequency of the excitation force ω or the frequency radio ω/Ω_n. Figure 11 shows the amplitude ratio of the boring bar with a certain frequency ratio ω/Ω_n. The frequency ratio is divided into six parts, 0.05–0.2, 0.25–0.45, 0.5–0.6, 0.7–1.0, 1.1–1.25, and 1.3–2.4, corresponding to Figures 11(a)–11(f). It is easy to find that, for some special frequency ratio bands, the amplitude ratio is always greater than 1, which means that regardless of how the parameters are adjusted, the dynamic displacement of the boring bar is always greater than the static displacement. For this reason, these frequency bands should be avoided as much as possible when selecting the cutting parameters in engineering. However, when these frequency bands cannot be avoided in engineering, we should also choose a reasonable DVA stiffness to make the amplitude ratio as low as possible. It can be seen that, among different ranges of frequency ratios, the amplitude ratio shows a completely different law of change. In Figure 11(a), the amplitude ratio decreases with increasing stiffness of the DVA; therefore, the stiffness of the DVA should be selected to be as large as possible. In this range of frequency ratios, the curves are almost straight lines, indicating that the amplitude ratio is not sensitive to the stiffness of the DVA. Therefore, if the rubber bush is not able to provide a sufficiently large stiffness, it is also possible to use a slightly lower stiffness. In Figure 11(b), the maximum point of the curve lies inside the stiffness range, and those maximum points should be avoided when selecting the cutting parameters. Moreover, compared to the response of the high-stiffness region, in the low-stiffness region, the amplitude ratio is lower, which means a low stiffness is more advantageous for obtaining stable cutting. In Figure 11(c), some minimum points can be found whose amplitude ratio is less than 1; if the boring bar can work at those minimum points, the vibration can be suppressed effectively. The curves in Figure 11(d) are similar to the curves in Figure 11(a). However, the slope is larger, which means that the amplitude ratio is sensitive to the stiffness, but by selecting a large stiffness of the DVA, the amplitude ratio can still be effectively controlled. The curves in Figure 11(e) are similar to the curves in Figure 11(b), but not all the curves obtain the best vibration suppression effect in the low-stiffness area. When the frequency ratio is 1.1 and 1.15, a higher stiffness is more beneficial for suppressing vibration. Conversely, when the frequency ratio is 1.2 and 1.25, a lower stiffness is more beneficial for suppressing vibration. The curves in Figure 11(f) have completely opposite law to the curves in Figures 11(a) and 11(d); the amplitude ratio increases with increasing stiffness of the DVA; therefore, the stiffness of the DVA should be selected to be as low as possible.

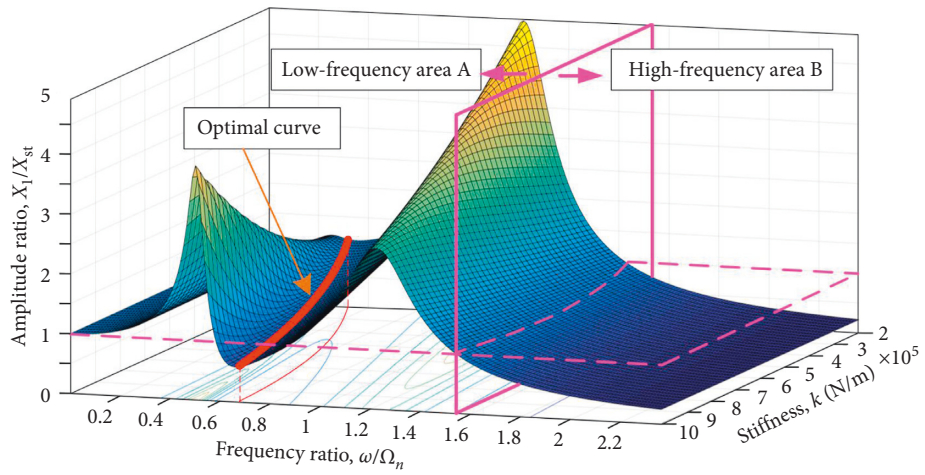

Figure 9: Three-dimensional surface of the amplitude ratio under the influence of the coupling of the frequency ratio and stiffness.

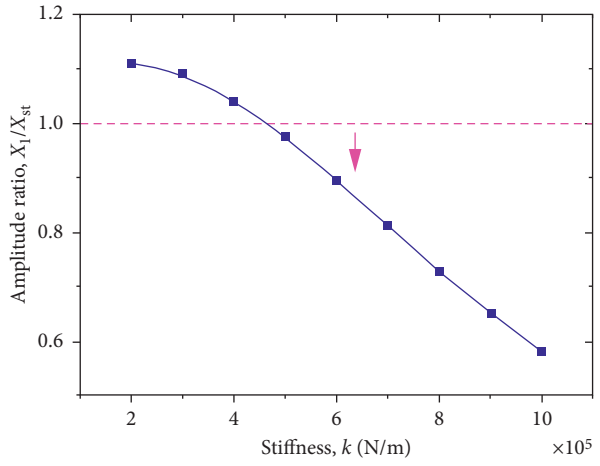

Figure 10: Amplitude ratio of the optimal curve.

From the above analysis, it is easy to see that the stiffness of the DVA has an important influence on the vibration suppression effect of the boring bar. Then, adjusting the rubber bushing in engineering to meet the requirements becomes an important issue.

4. Analysis of the Stiffness of the DVA

As shown in Figure 1, the stiffness of the DVA is provided by two rubber bushes. The vibration causes the mass block to vibrate in the radial direction. The radial stiffness of the DVA can be adjusted by rotating the knob at the end of the DVA (as shown in Figure 1) to change the compression s_{DVA} (as shown in Figure 12) in the axial direction. When the knob is turned clockwise, s_{DVA} increases, and then the radial stiffness of the DVA also increases. Conversely, if the knob is turned counterclockwise, s_{DVA} decreases, and the radial stiffness of the DVA also decreases. Therefore, the key to the problem is to find the relationship between the radial stiffness and axial compression s_{DVA}. For this purpose, the finite element analysis and experiment are conducted as follows.

The finite element model of a single rubber bush is established in Abaqus, as shown in Figure 12. Using reduced-integration hybridization elements, a total of 25636 elements were obtained. The inner cylinder is fixed, while the outer cylinder can move in the axial direction. By changing the axial compression s, the axial compression can be adjusted. A force F is loaded on the outer cylinder to create a displacement d, and then the radial stiffness of a single rubber bush can be obtained:

$$k_{\text{single}} = \frac{F}{d}. \tag{18}$$

As there are two rubber bushes placed parallel inside the DVA, the stiffness of the DVA can be calculated by

$$k = 2k_{\text{single}}. \tag{19}$$

To make the simulation accurate, it is important to find the parameters of the rubber bush. Since the parameters of the rubber material are inconvenient to measure directly, it is better to reverse the parameters from experimental results. Since the formula for calculating the radial stiffness of the rubber bush is not yet mature but the formula for calculating the axial stiffness of the rubber bush has been widely used [25], the axial stiffness test is used to extract the parameters. The axial compression experiment is carried out as shown in Figure 13. A load is applied in the axial direction, and then the axial stiffness can be obtained by constructing the force-displacement curve.

The axial stiffness of a rubber bush can be expressed by the following equation [25]:

$$k_a = E_a \frac{\pi\left(D^2 - d^2\right)}{4h}, \tag{20}$$

where D, d, and h are the outer diameter, inner diameter, and height of the rubber bush, respectively, and E_a is the appropriate apparent Young's modulus:

$$E_a = iG, \tag{21}$$

where $i = 3.6(1 + 1.65S^2)$ is the geometric shape factor for an annular rubber bush and $S = (D - d)/4h$ is the area ratio

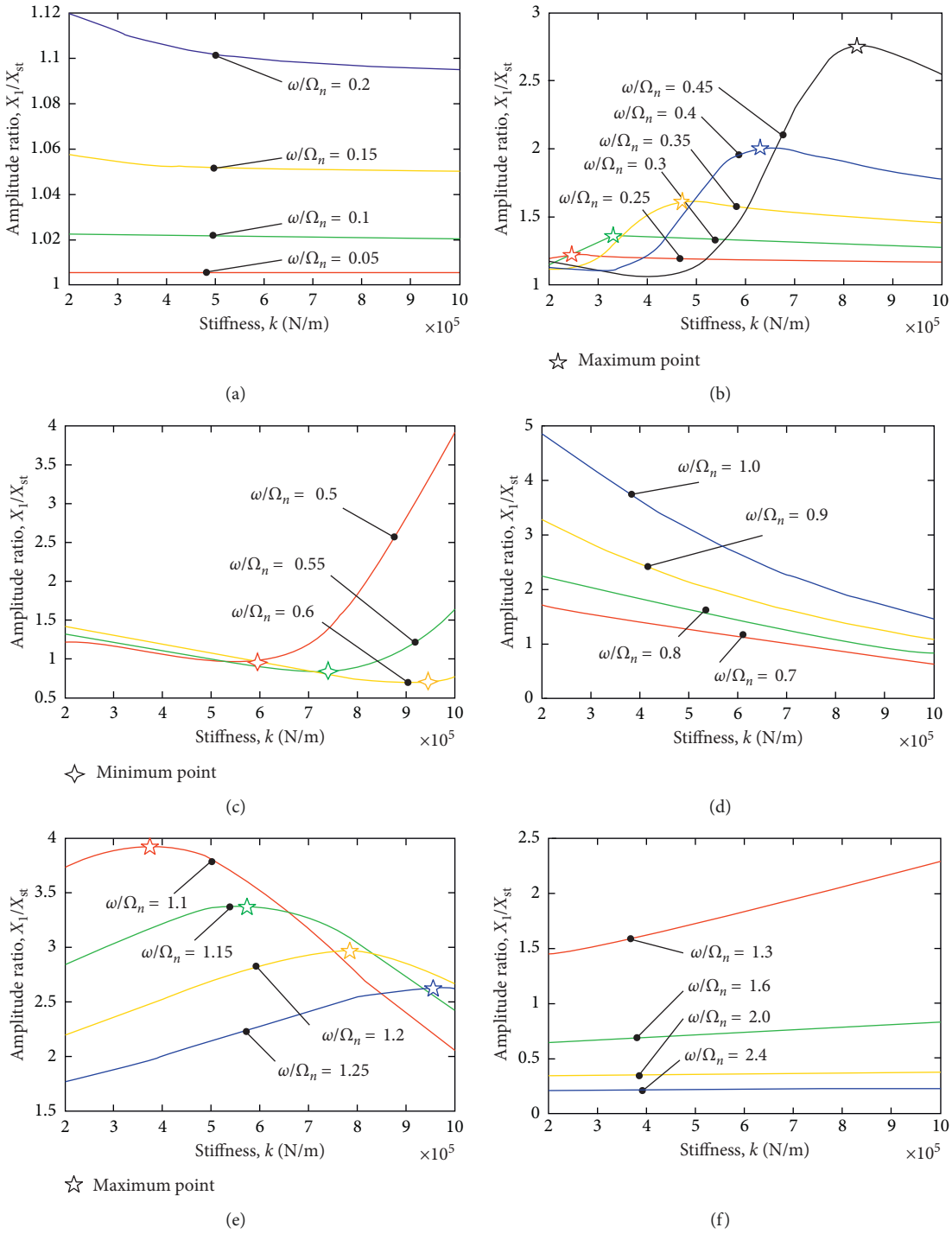

FIGURE 11: Amplitude ratio of the boring bar for certain frequency ratios. Frequency ratios: (a) 0.05–0.2; (b) 0.25–0.45; (c) 0.5–0.6; (d) 0.7–1.0; (e) 1.1–1.25; (f) 1.3–2.4.

of the loaded surface to the force-free surface. Young's modulus $E = 3E_a$.

Then, the parameters of the rubber bush can be obtained, as shown in Table 2.

By substituting the parameter values in Table 2 into the finite element model and selecting different axial compression values s, the force-displacement curve of the rubber bush can be obtained, and then the radial stiffness can be obtained by deriving the force-displacement curve. It is worth noting that since a DVA contains two rubber bushes, the axial compression s of a single rubber bush is only half of the DVA's axial compression:

$$s_{DVA} = 2s. \tag{22}$$

The experiment of the radial stiffness of the DVA is also carried out to verify the simulation results, as shown in

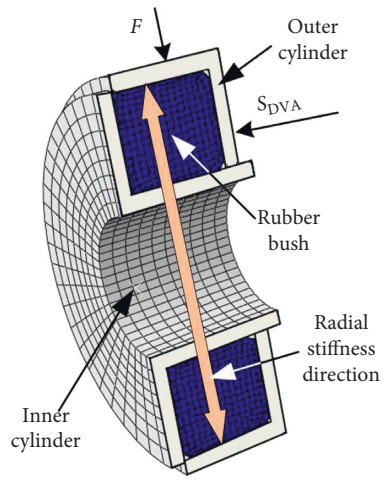

Figure 12: Finite element model of a single rubber bush.

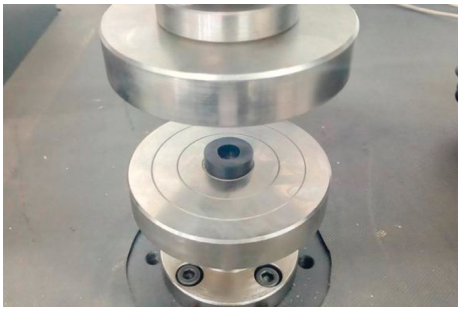

Figure 13: Axial compression experiment of the rubber bush.

Table 2: Parameters of the rubber bush.

D (mm)	d (mm)	h (mm)	E_a (MPa)	E (MPa)
24.2	11.5	7.1	0.5	1.5

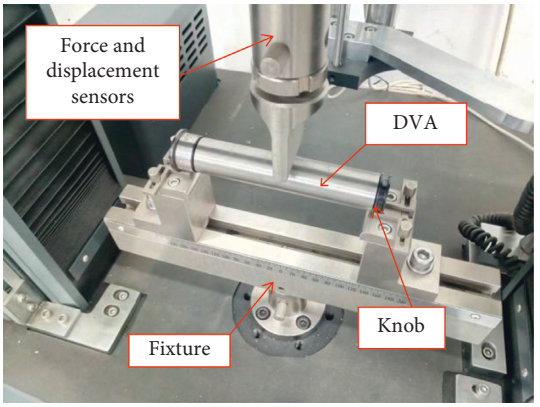

Figure 14: Experiment of the radial stiffness of the DVA.

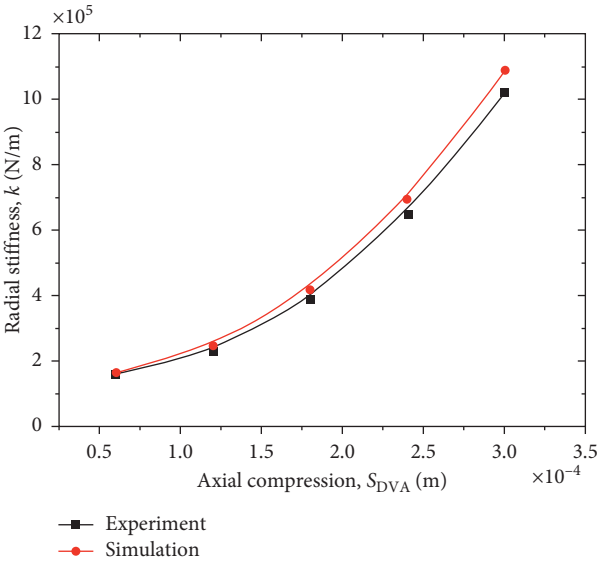

Figure 15: Experiment and simulation results of the stiffness of the DVA.

Figure 14. Figure 15 shows a comparison of the experimental and simulation results.

It can be seen that as the axial compression increases, the stiffness of the DVA increases nonlinearly. In addition, the simulation results are slightly larger than the experimental results. This condition occurs because, in the simulation, the inner and outer cylinders are set as rigid bodies, which means they have no deformations regardless

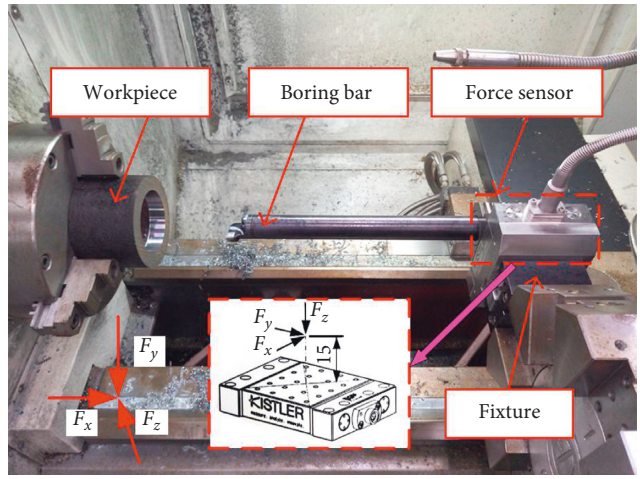

Figure 16: Boring experiment.

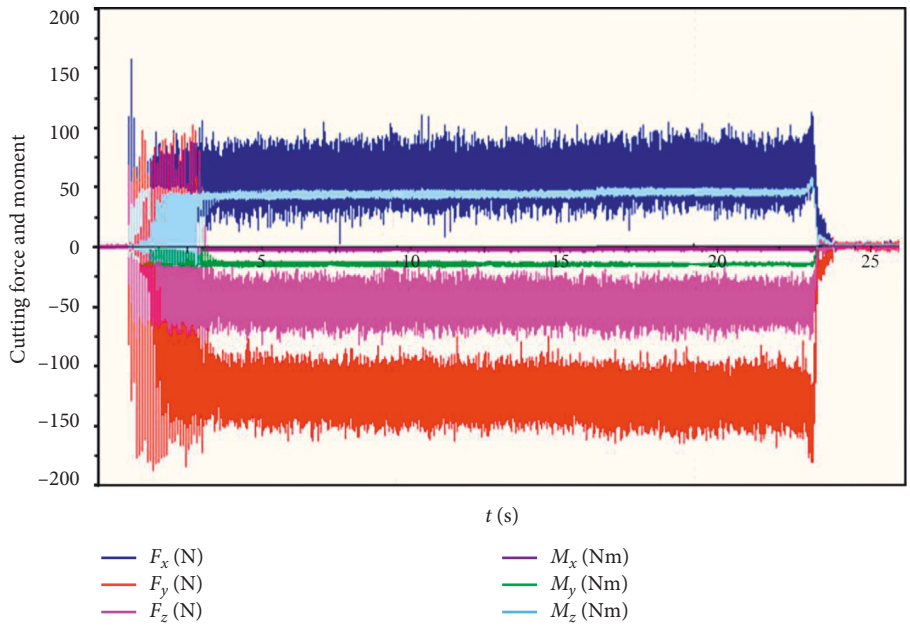

Figure 17: Stable states.

of how large the load is. However, the inner and outer cylinders are actually made of metal. Thus, in the experimental situation, they exhibit a slight deformation under load. This deformation is superimposed on the deformation of the rubber bush, resulting in the lower experimental result. However, even at the maximum compression, the error is still less than 5%.

Thus, the relationship between the radial stiffness and axial compression of the DVA has been established, and then, the relationship between the amplitude ratio and the axial compression can be established indirectly. In engineering, we first select the excitation frequency, then determine the optimal DVA stiffness, and finally obtain the corresponding axial compression. By selecting the appropriate axial compression, the boring bar can work in a stable state.

5. Boring Experiments

The boring experiments were carried out to analyze the vibration suppression effect of the boring bar with a variable stiffness DVA. As shown in Figure 16, the workpiece is a hollow cylinder with an inner diameter of 100 mm and an outer diameter of 160 mm; the material is C45E4. The cutting force and moment are detected by a dynamometer from Kistler (type: 9129AA).

The excitation frequency can be adjusted by changing the spindle speed. The stable and unstable states can be evaluated by comparing the values of the cutting force and moment. Figures 17 and 18 show the cutting force and moment of stable and unstable states, respectively. Table 3 shows the statistical results of the cutting force and moment. It can be seen that when the boring works in a stable state, the

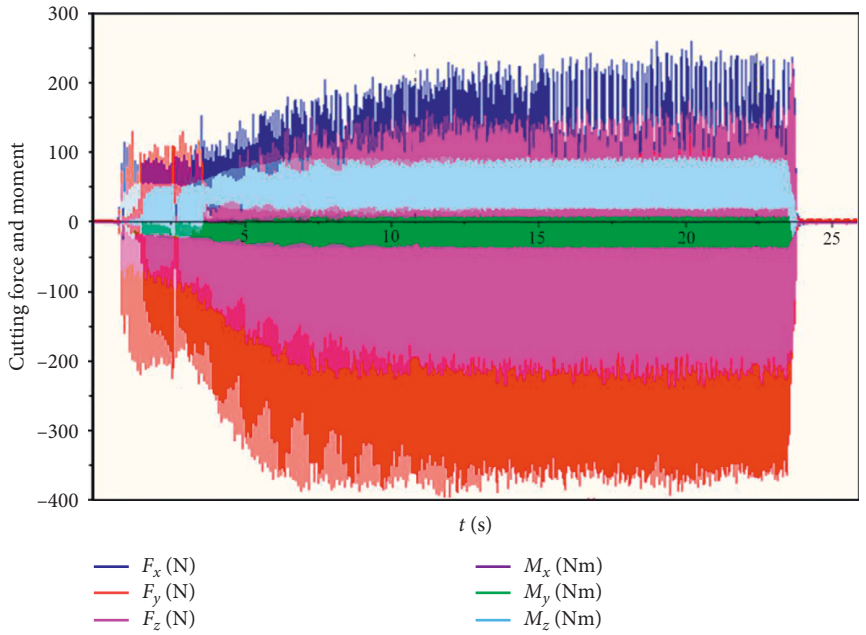

Figure 18: Unstable states.

Table 3: Statistical results of the cutting force and moment of the stable and unstable states.

States		F_x (N)	F_y (N)	F_z (N)	M_x (Nm)	M_y (Nm)	M_z (Nm)
Stable	Min.	8.270	−163.20	−82.96	−4.738	−17.51	39.51
	Max.	110.0	−75.12	−10.99	−0.430	−12.01	48.75
	Amplitude	50.9	44.04	35.99	2.154	2.75	4.62
Unstable	Min.	−153.0	−398.8	−238.6	−14.09	−37.60	14.37
	Max.	261.3	129.4	174.7	7.461	9.256	96.8
	Amplitude	207.2	264.1	206.7	10.78	23.43	41.22
	Amplitude increase radio	307%	500%	474%	400%	752%	792%

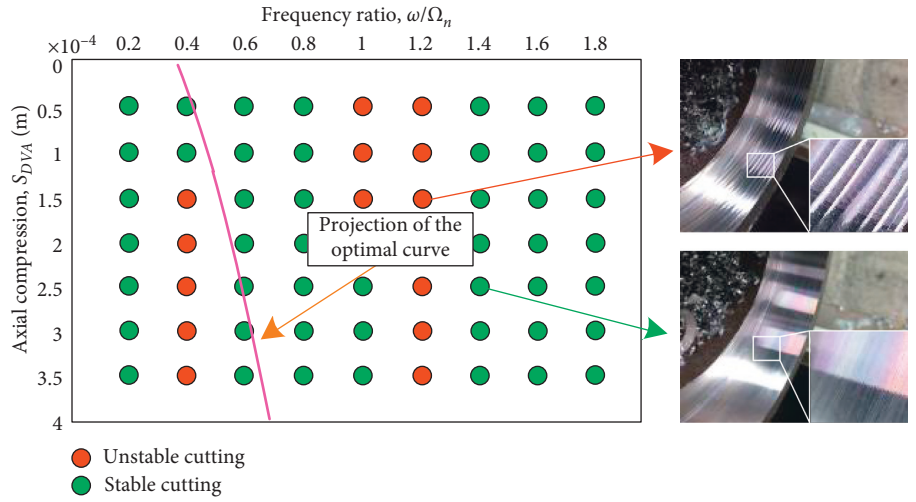

Figure 19: Stable and unstable cutting experiment results.

amplitude is small, and every curve can be clearly distinguished. However, when the boring works in an unstable state, the amplitude is large, causing all the curves to overlap. As mentioned before, the tangential force F_c and radial force F_p have the most important influence on chip thickness variation, so in Table 3, the amplitude increase radio for the tangential F_y and radial forces F_z are larger than the axial force F_x.

Figure 19 shows the stable and unstable cutting experiment results; it can be seen the cutting stable states can be adjusted by changing the axial compression s_{DVA} of the DVA at different frequency ratios. The stiffness of the DVA changes along with the axial compression. For example, when the frequency ratio is approximately 0.4, it is better to use a small axial compression, while when the frequency ratio is approximately 1, it is better to use a large axial compression. However, when the frequency ratio is approximately 1.2, the boring bar always works in an unstable state. This frequency ratio should be avoided when selecting the spindle speed. The pink line in Figure 19 corresponds to the projection of the optimal curve in Figure 9. When the boring bar's cutting parameters are selected close to the optimal curve, the boring bar can work at a stable state, verifying the rationality of the previous modeling and analysis. The experimental results indicate that the boring bar with a variable stiffness DVA can suppress the vibration over a larger excitation frequency range. By changing the axial compression s_{DVA} of the DVA, the boring bar can work at a stable state.

6. Conclusions

The vibration characteristics of the boring bar with a variable stiffness DVA are investigated. A two-degree-of-freedom dynamic model is established, and the parameters measured through the experiment are submitted to the kinetic equation to analyze the vibration characteristics of the boring bar. The vibration characteristics of the boring bar with a variable stiffness DVA and those of the regular boring bar without a DVA are compared, and the result shows that the boring bar with a variable stiffness DVA has a better vibration reduction effect. In addition, the amplitude ratio of the boring bar differs greatly by changing the stiffness of the DVA; only in certain frequency ranges can the amplitude ratio be less than 1. The entire frequency ratio area, in the range of 0–2.2, is divided into two parts: the low-frequency area A and the high-frequency area B. The dividing line is located at a frequency ratio of approximately 1.55. In area B, the boring bar can always have the effect of vibration reduction, but in area A, there are two ridges where the amplitude ratio is very high. In the valley between the two ridges, an optimal curve can be found in the frequency range 0.4–0.8, where the amplitude ratio is less than 1. In previous studies, the purpose of optimization has been to equalize the heights of the two peaks over a large excitation frequency range. However, in engineering practice, the excitation frequency is generally a certain value for a specific processing condition. This means that making two peaks equal in height cannot provide the optimal parameter. Therefore, in engineering practice, the most important thing is to select the appropriate stiffness of the DVA according to the different frequencies of the excitation force; thus, in this paper, the amplitude ratio of the boring bar with a certain frequency ratio is studied. The frequency ratio is divided into six parts: 0.05–0.2, 0.25–0.45, 0.5–0.6, 0.7–1.0, 1.1–1.25, and 1.3–2.4. With different frequency ratios, the amplitude ratio shows a completely different law of change, but by selecting a certain stiffness of the DVA, the vibration can be effectively suppressed. It is worth noting that how to achieve the stiffness value by engineers is what we focus on mostly. Therefore, this paper establishes the relationship between the theoretical stiffness value and the axial compression. The stiffness of the DVA is provided by the radial stiffness of two rubber bushes equipped inside the DVA. By changing the axial compression of the DVA, the radial stiffness of the rubber bushes is changed; at the same time, the stiffness of the DVA is also changed. Then, the simulations and experiments focusing on the stiffness of the DVA are conducted to establish the relationship between the axial compression and the stiffness. By selecting the appropriate axial compression, the boring bar can work under the steady state. Finally, a boring experiment with different axial compressions of the DVA is conducted to detect the stable and unstable states. The results show that when the boring bar works in an unstable state, the amplitude increase ratio of the cutting force and the moment, especially for the tangential F_y and radial forces F_z increases substantially. The experimental results verify the accuracy of the previous modeling and analysis. Based on this research, in engineering practice, we first select the excitation frequency, then determine the optimal DVA stiffness, and finally obtain the corresponding axial compression. By changing the axial compression of the DVA, the boring bar can cut at a stable state, which can guide the parameter implementation in engineering application.

Data Availability

The data used to support the findings of this study are included within the article.

Conflicts of Interest

The authors declare that they have no conflicts of interest.

Acknowledgments

This research was funded by the Fundamental Research Funds for the Central Universities (grant no. KYLX16_0186) and the National Science and Technology Major Project (grant no. 2013ZX04012032).

References

[1] M. Siddhpura and R. Paurobally, "A review of chatter vibration research in turning," *International Journal of Machine Tools and Manufacture*, vol. 61, pp. 27–47, 2012.

[2] G. Quintana and J. Ciurana, "Chatter in machining processes: a review," *International Journal of Machine Tools and Manufacture*, vol. 51, no. 5, pp. 363–376, 2011.

[3] A. Som, D.-H. Kim, and H. Son, "Semiactive magneto-rheological damper for high aspect ratio boring process," *IEEE/ASME Transactions on Mechatronics*, vol. 20, no. 5, pp. 2575–2582, 2015.

[4] J. R. Pratt and A. H. Nayfeh, "Chatter control and stability analysis of a cantilever boring bar under regenerative cutting conditions," *Philosophical Transactions of the Royal Society of*

London. Series A: Mathematical, Physical and Engineering Sciences, vol. 359, no. 1781, pp. 759–792, 2001.

[5] X. Lei and C. Wu, "Investigating the optimal damping performance of a composite dynamic vibration absorber with particle damping," *Journal of Vibration Engineering & Technologies*, vol. 6, no. 6, pp. 503–511, 2018.

[6] D. I. Suyama, A. E. Diniz, and R. Pederiva, "The use of carbide and particle-damped bars to increase tool overhang in the internal turning of hardened steel," *International Journal of Advanced Manufacturing Technology*, vol. 86, no. 5–8, pp. 2083–2092, 2016.

[7] F. Xia, Z. Q. Liu, and Q. H. Song, "Boring bar with constrained damping," *Acta Aeronautica et Astronautica Sinica*, vol. 35, no. 9, pp. 2652–2659, 2014.

[8] M. Sortino, G. Totis, and F. Prosperi, "Development of a practical model for selection of stable tooling system configurations in internal turning," *International Journal of Machine Tools and Manufacture*, vol. 61, pp. 58–70, 2012.

[9] L. Houck III, T. L. Schmitz, and K. Scott Smith, "A tuned holder for increased boring bar dynamic stiffness," *Journal of Manufacturing Processes*, vol. 13, no. 1, pp. 24–29, 2011.

[10] X. Liu, Q. Liu, S. Wu, R. Li, and H. Gao, "Analysis of the vibration characteristics and adjustment method of boring bar with a variable stiffness vibration absorber," *International Journal of Advanced Manufacturing Technology*, vol. 98, pp. 95–105, 2018.

[11] X. Liu, Q. Liu, S. Wu, R. Li, and H. Gao, "Research on the performance of damping boring bar with a variable stiffness dynamic vibration absorber," *International Journal of Advanced Manufacturing Technology*, vol. 89, no. 9–12, pp. 2893–2906, 2017.

[12] L. Li and B. Sun, "Optimal parameters selection and engineering implementation of dynamic vibration absorber attached to boring bar," in *Proceedings of the INTER-NOISE and NOISE-CON Congress and Conference Proceedings*, Hamburg, Germany, August 2016.

[13] L. Rubio, J. A. Loya, M. H. Miguelez, and J. Fernandez-Saez, "Optimization of passive vibration absorbers to reduce chatter in boring," *Mechanical Systems and Signal Processing*, vol. 41, no. 1-2, pp. 691–704, 2013.

[14] M. H. Miguélez, L. Rubio, J. A. Loya, and J. Fernández-Sáez, "Improvement of chatter stability in boring operations with passive vibration absorbers," *International Journal of Mechanical Sciences*, vol. 52, no. 10, pp. 1376–1384, 2010.

[15] M. Sortino, G. Totis, and F. Prosperi, "Modeling the dynamic properties of conventional and high-damping boring bars," *Mechanical Systems and Signal Processing*, vol. 34, no. 1-2, pp. 340–352, 2013.

[16] E. Budak and E. Ozturk, "Dynamics and stability of parallel turning operations," *CIRP Annals*, vol. 60, no. 1, pp. 383–386, 2011.

[17] U. Yigit, E. Cigeroglu, and E. Budak, "Chatter reduction in boring process by using piezoelectric shunt damping with experimental verification," *Mechanical Systems and Signal Processing*, vol. 94, pp. 312–321, 2017.

[18] E. Abele, M. Haydn, and T. Grosch, "Adaptronic approach for modular long projecting boring tools," *CIRP Annals*, vol. 65, no. 1, pp. 393–396, 2016.

[19] Y. Alammari, M. Sanati, T. Freiheit, and S. S. Park, "Investigation of boring bar dynamics for chatter suppression," *Procedia Manufacturing*, vol. 1, pp. 768–778, 2015.

[20] F. Chen, M. Hanifzadegan, Y. Altintas, and X. Lu, "Active damping of boring bar vibration with a magnetic actuator," *IEEE/ASME Transactions on Mechatronics*, vol. 20, no. 6, pp. 2783–2794, 2015.

[21] X. Lu, F. Chen, and Y. Altintas, "Magnetic actuator for active damping of boring bars," *CIRP Annals*, vol. 63, no. 1, pp. 369–372, 2014.

[22] F. Chen, X. Lu, and Y. Altintas, "A novel magnetic actuator design for active damping of machining tools," *International Journal of Machine Tools and Manufacture*, vol. 85, pp. 58–69, 2014.

[23] A. Matsubara, M. Maeda, and I. Yamaji, "Vibration suppression of boring bar by piezoelectric actuators and LR circuit," *CIRP Annals*, vol. 63, no. 1, pp. 373–376, 2014.

[24] I. Lazoglu, F. Atabey, and Y. Altintas, "Dynamics of boring processes: part III-time domain modeling," *International Journal of Machine Tools and Manufacture*, vol. 42, no. 14, pp. 1567–1576, 2002.

[25] L. Li, B. Sun, M. He, and H. Hua, "Analysis of the radial stiffness of rubber bush used in dynamic vibration absorber based on artificial neural network," *NeuroQuantology*, vol. 16, no. 6, pp. 737–744, 2018.